Preparation and Characterization of the *Bombyx mori* Silk Fibroin Solution

Karan Khurana
MS12074

A dissertation submitted for the partial fulfilment of BS-MS dual degree in Science

Indian Institute of Science Education and Research Mohali
April, 2017

Certificate of Examination

This is to certify that the dissertation titled **"Preparation and Characterization of the *Bombyx mori* Silk Fibroin Solution"** submitted by **Karan Khurana** (Reg. No. MS12074) for the partial fulfillment of BS-MS dual degree programme of the Institute, has been examined by the thesis committee duly appointed by the Institute. The committee finds the work done by the candidate satisfactory and recommends that the report be accepted.

Dr. Abhishek Chaudhuri | Dr. Sanjeev Kumar | Dr. Kamal P. Singh (Supervisor)

Dated: April 21, 2017

Declaration

The work presented in this dissertation has been carried out by me under the guidance of Dr. Kamal P. Singh at the Indian Institute of Science Education and Research Mohali.

This work has not been submitted in part or in full for a degree, a diploma, or a fellowship to any other university or institute. Whenever contributions of others are involved, every effort is made to indicate this clearly, with due acknowledgement of collaborative research and discussions. This thesis is a bonafide record of original work done by me and all sources listed within have been detailed in the bibliography.

Karan Khurana
(Candidate)

Dated: April 21, 2017

In my capacity as the supervisor of the candidate's project work, I certify that the above statements by the candidate are true to the best of my knowledge.

Dr. Kamal P. Singh
(Supervisor)

Dated: April 21, 2017

Acknowledgement

I would like to express the deepest appreciation to my supervisor, Dr. Kamal P. Singh for his unceasing support throughout my MS thesis. I would like to thank him for his guidance, patience, motivation, enthusiasm, and immense knowledge. Without his guidance and persistent help this dissertation would not have been possible.

I would like to express my sincere gratitude to Dr. M. S. Sidhu and Dr. Gopal Verma for their endless assistance, motivation and insightful comments. I would like to thank Komal Chaudhary, Gyanendra Yadav for helping me with the Liquid Drop Interferometer (LDI) technique and letting me use their set-up. I would also like to thank all the members of the Femtosecond Laser lab for providing a positive and enthusiastic work environment.

I would also like to extend my thanks to Dr. Samrat Mukhopadhyay for the Raman Spectrometer and Bhavin Kansara for helping me with the instrument, Professor Sanjay Mandal and Sandeep Kashyap for doing the Powder X-Ray diffraction and Mayank Saraswat for helping me with UV-Vis spectrometer.

Last but not the least, I would like to thank my family: my parents and my sister for their continuous and unparalleled love, help and support.

List of Figures

List of Tables

Notations

LDI	:	Liquid Drop Interferometer.
BS	:	Beam Spliter.
M	:	Mirror.
L	:	Lens.
BS	:	Beam Splitter.
PD	:	Photodiode.
UV	:	Ultraviolet.
MWCO	:	Molecular Weight Cut-Off.
FWHM	:	Full Width at Half Maximum.
PXRD	:	Powder X-Ray Diffraction.

Contents

"*Nothing in life is to be feared, it is only to be understood. Now is the time to understand more, so that we may fear less.*"

– Marie Curie

Abstract

Silk fibroin has been proven to be a remarkable biomaterial and various material formats such as thin films, sponges, hydrogels, thin tubes, electrospun fibers have been processed from it. In this thesis, we extracted fibroin from the silk cocoons to make aqueous solution of the silk and used it in characterization of *bombyx mori* silk fibroin by using techniques like Raman spectroscopy, Ultraviolet–visible spectroscopy and X-ray diffraction crystallography. We used this solution to study the nanoscale deformations in the silk drop with time using pump-probe technique on Liquid Drop Interferometer set-up. Both radiation pressure effect, in agreement with Minkowski's momentum, and thermal effect were observed on the silk drop. We calculated change in surface tension and thermal diffusivity using radiation pressure effect and thermal effect, respectively.

Chapter 1

Protocol for Preparing Aqueous Silk Solution from *Bombyx mori* Silk Cocoons

1.1 Introduction

Silk fibroin has been proven to be a remarkable biomaterial due to its robust mechanical properties, biocompatibility, high permeability to oxygen gas [1, 2], its versatility in processing into many material formats and ease with which it can be chemically modified [3, 4]. Furthermore, degradation rates of these silk protein materials can also be controlled based on the processing conditions [5, 6, 7], which impact crystallinity of the material. To process the silk into different materials, we need to prepare aqueous solution of the silk. This regenerated silk solution can then be reformed into a variety of three-dimensional geometries [4].

In this chapter, we prepared an aqueous silk solution by reproducing the protocol published by Rockwood et al. in Nature Protocols [4]. We did fine tuning in the protocol conditions depending upon our silk and the available equipment.

1.1.1 Silkworm silk

Silk is a fibrous protein, synthesized in the epithelial cells in the glands of spiders and several worms of the order Lepidoptera. It is one of the most useful and oldest natural fiber in the world with an evolutionary history of over 380 million years [8]. Silkworm silk is highly regarded in the textile industry for its lustre and mechanical properties. Commercial silkworm *Bombyx mori* has been cultivated by man for centuries. Silkworm silk is obtained from the cocoons spun by the silkworms. Silkworm cocoon has a non-woven structure made

of continuous silk fibres stuck together by the glu-like protein sericin. Silk fibres that are spun into cocoons are in the form of a bave, i.e. a pair of fibroin brins with sericin covering [9]. A silkworm cocoon mainly consists of two proteins, fibroin and sericin. Fibroin content is about 70% and sericin content is about 30% [10]. As a biological structural material, it has a hierarchical structure that has been optimized through evolutionary pressures over millions of years.

Figure 1.1: *Bombyx mori* larvae [Author: Fastily, Source: Wikipedia], silk cocoon, pupae and adult silkworm moth [Author: Oakenking, Source: Wikipedia]

1.1.2 Structure of the silk fibroin

Bombyx mori silk fibroin consists of 16 amino acids [10] (Table 1.1) with a mean molecular weight of 350 kDa. The combined mole fraction of glycine, alanine and serine is 85% [10], and therefore, silk fibroin molecule of *Bombyx mori* primarily consists of highly repetitive sequence, Gly–Ala–Gly–Ala–GLy –Ser [11, 12].

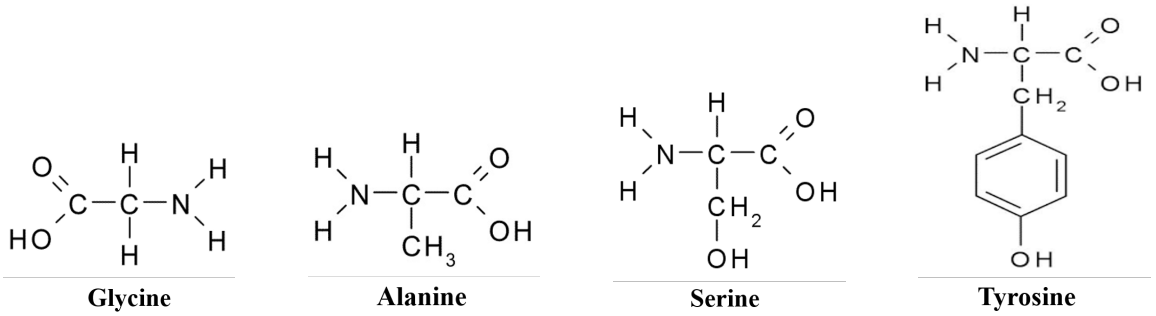

Figure 1.2: Chemical structures of the amino acids present in silk fibroin. Mole fraction of glycine, alanine, serine, tyrosine combined is about 90%.

Table 1.1: Amino acid composition of the *Bombyx mori* silk fibroin

Amino acid	**Mol %**
Glycine	42.9
Alanine	30.0
Serine	12.2
Tyrosine	4.8
Valine	2.5
Aspartic acid	1.9
Glutamic acid	1.4
Threonine	0.92
Phenylalanine	0.67
Isoleucine	0.64
Leucine	0.55
Arginine	0.51
Proline	0.45
Lysine	0.38
Methionine	0.37
Histidine	0.19

Secondary structure of fibroin is stabilized by various kinds of interactions. Interchain hydrogen bonds between functional groups of peptide macrochains, intrachain hydrogen bonds between side fragments of macromolecules, dipolar interactions due to polar carboxy and amino groups and van der Waals forces.

There are four kinds of secondary structures present in silk fibroin:

- α-helical structures (Figure 1.3)
- β-folded structures (Figure 1.3)
- Turns
- Disordered conformations of random globules

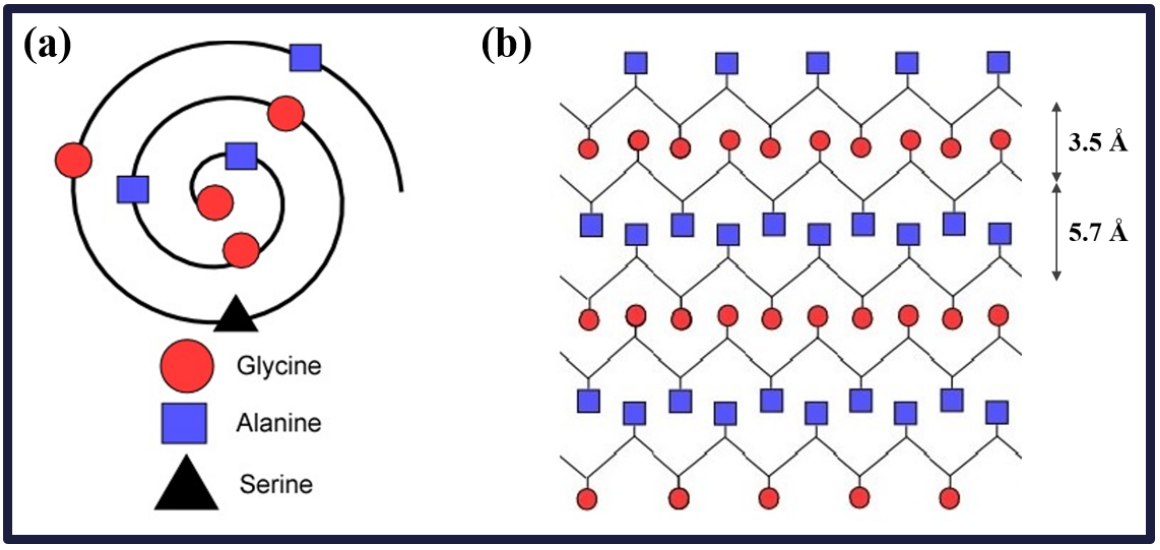

Figure 1.3: Secondary structures of silk fibroin: (a) α-helical with repeating sequence Gly–Ala–Gly–Ala–GLy–Ser. (b) Antiparallel β-sheets with repeated Gly–Ala sequence.

α-helical structure (Figure 1.3) is formed by intermolecular hydrogen bonds, with the hydrophobic fragments displaced to the periphery [13]. In β-folded structure, the macromolecules are arranged in the parallel or antiparallel mode, forming a folded sheet or layerd β-sheets. Antiparallel β-sheets (Figure 1.3) of silk fibroin are packed in the face-to-face, back-to-back mode [11]. For the hydrophobic fragments of macromolecules, this structure is the most favorable energetically [14, 15].

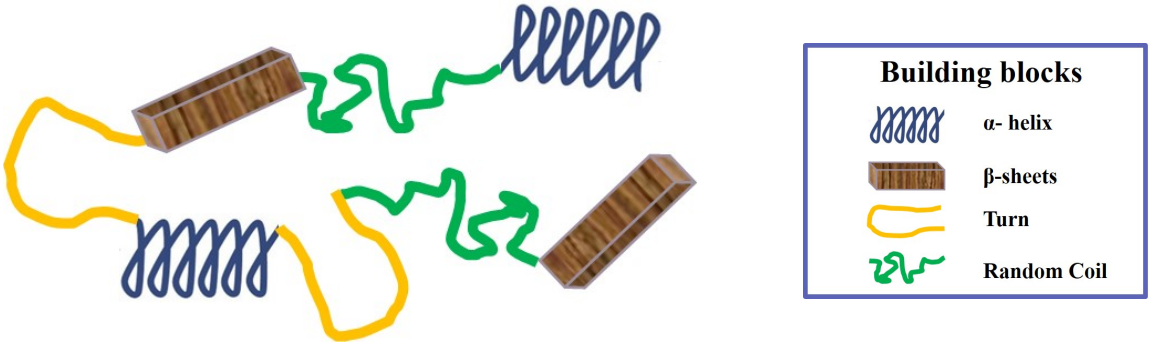

Figure 1.4: Schematic diagram illustrating the silk protein tertiary structure.

1.1.3 Type of silks

Fibroin arrange itself in three structures, called silk I, silk II, and silk III

- **Silk I** is the natural form of fibroin, as emitted from the *Bombyx mori* silk glands. It is poorly defined and mostly consists of extended helices and random coils.
- **Silk II** is the fibroin in spun silk. It consists of β-sheets which impart it with greater mechanical strength.
- **Silk III** found principally in solutions of fibroin at an interface (i.e. air-water interface, water-oil interface, etc.) [16].

1.2 Procedure

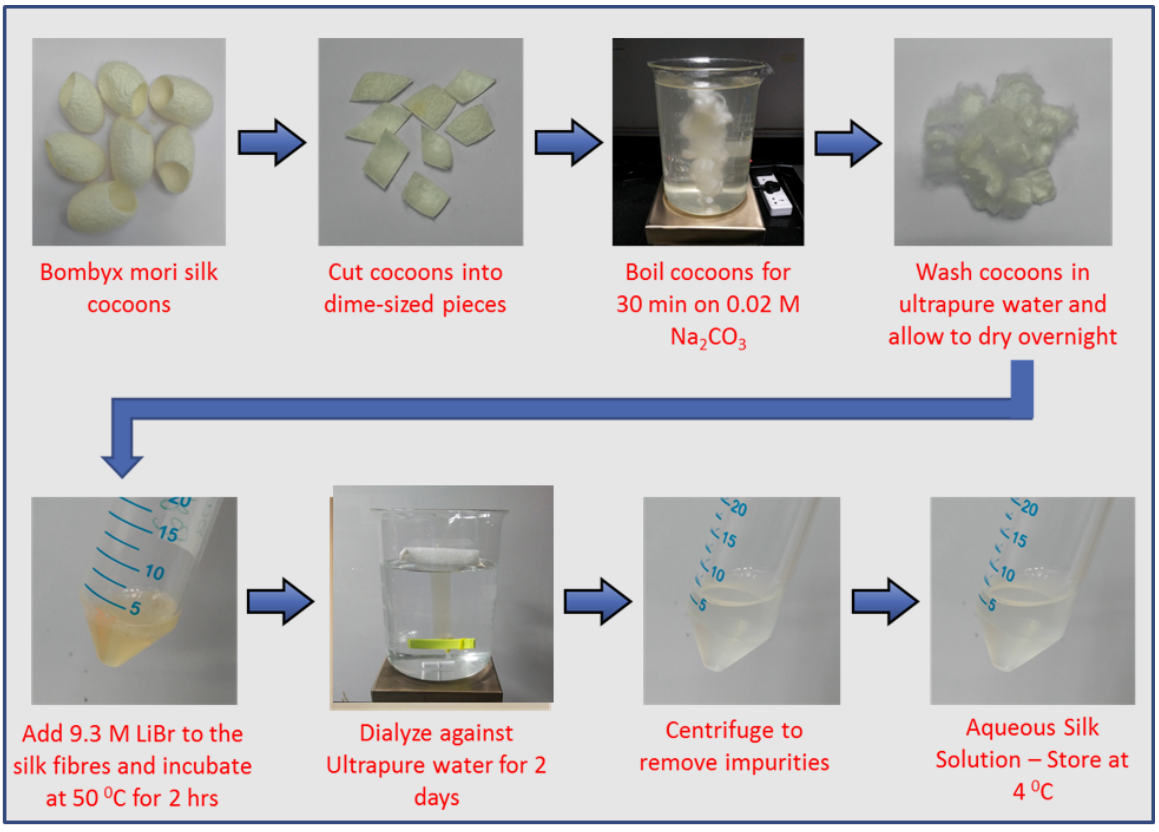

Figure 1.5: Schematic for preparing silk fibroin solution from the *Bombyx mori* silk cocoons. Complete process takes 4 days.

1.2.1 Step I: Removal of sericin protein from the silkworm cocoons

First step in the protocol is to remove the glue-like protein sericin from the cocoons. Sericin covers the surface of the silk filament core protein, fibroin. Na_2CO_3 solution, like soap solution, removes the glue-like protein. Weight of the silk gets reduced by nearly 30% after removing the sericin. Procedure mentioned below is designed for 5 g of silk cocoons. If more material is required, the volumes can be scaled appropriately.

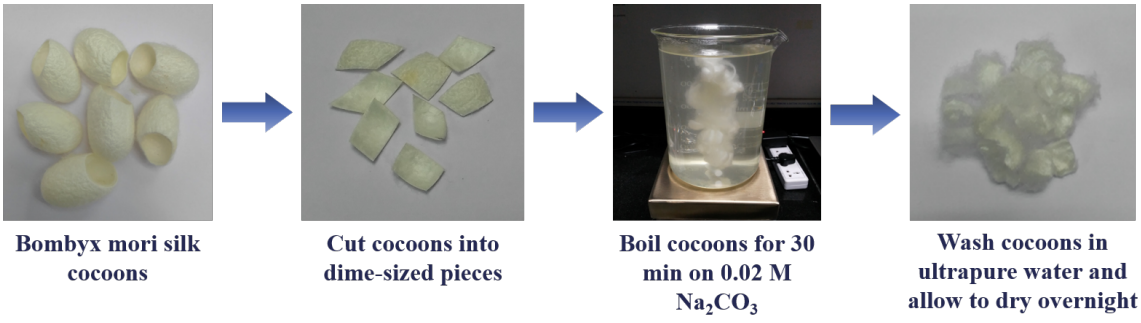

Figure 1.6: Procedure for removing glue-like protein, *sericin form the silkworm cocoons.*

PROCEDURE

1. Cut the silk cocoons into small pieces. Weigh out 5 g of the cocoon pieces.
2. Fill a glass beaker with 2 L of ultrapure water and cover it with aluminum foil.
3. Place the glass beaker on the hot plate and heat until boiling.
4. When water starts boiling, add 4.24 g (105.9888 $g/mol \times 0.02\ mol/l \times 2\ l$) of Na_2CO_3 to prepare 0.02 M Na_2CO_3 solution.
5. Once the solution starts to boil, add cocoon pieces and continue boiling for 20 min while gently stirring on the magnetic stirrer.
6. Remove the silk fibroin and wash it with ultrapure water. Squeeze excess water out of the fibers.
7. Fill a glass beaker with utrapure water and place silk fibroin in it with a stir bar. Rinse the fibroin in ultrapure water for 5 min while gently stirring.
8. Repeat steps 6 and 7.
9. Remove the silk fibroin from water, squeeze it and spread it out on aluminum foil and let it dry.

1.2.2 Step II: Dissoution of silk fibroin in LiBr

Next step in the protocol is to dissolve silk fibroin in appropriate solvent. Various studies have shown various molecular and ionic solvents that can dissolve silk fibroin [4, ?]. We used 9.3 M LiBr as it exhibit high solvency. LiBr disrupts the high degree of hydrogen bonding that exists between the individual protein molecules [17, 18].

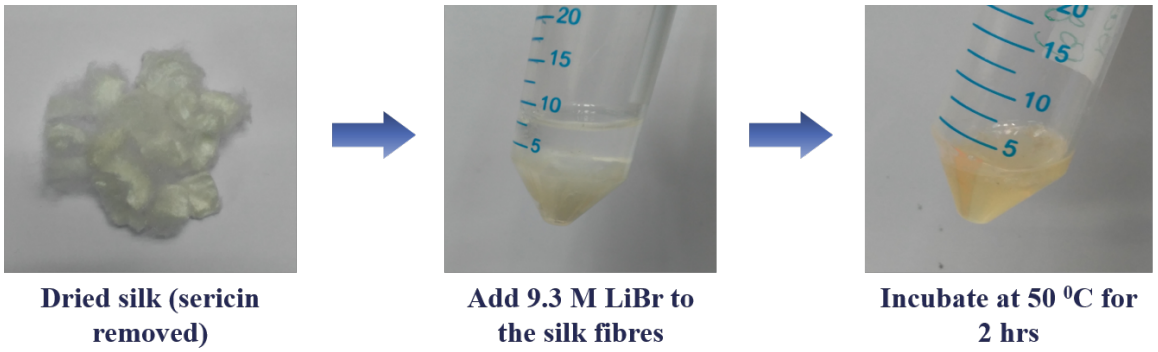

Figure 1.7: Procedure for dissolving silk fibroin in 9.3 M LiBr.

PROCEDURE

10. Weigh the dried silk fibroin obtained in the previous step.
11. Multiply the amount of dried silk fibroin by 4 to obtain the total volume of 9.3 M LiBr needed.
12. Prepare 9.3 M LiBr solution by slowly adding the required amount of LiBr with constant stirring and carrying this out on ice as adding LiBr to water is an exothermic process.
13. Pack silk fibroin in a conical tube and add the required amount of 9.3 M LiBr solution on top.
14. Place the conical tube in oven at 45 °C for 3 h.
15. Assess visually if there is any undissolved silk. If there is, then, keep the conical tube in the oven for more time.

1.2.3 Step III: Dialysis and centrifugation

To remove LiBr from the solution, the solution is dialyzed against ultrapure water for 2 days. Dialysis tube of MWCO 3.5 kDA is used. After dialysis, solution is centrifuged twice to any undissolved silk and impurities.

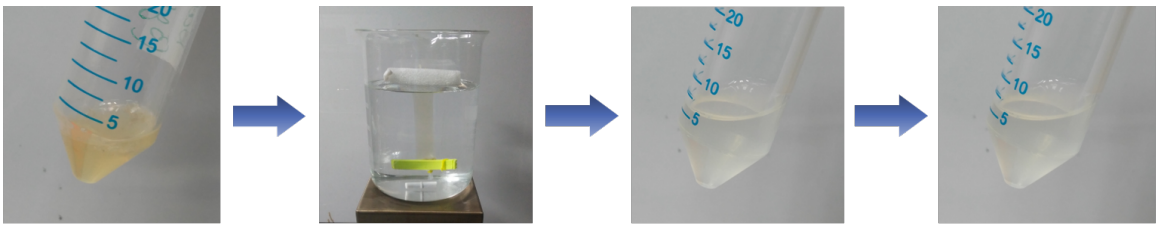

Figure 1.8: Dialysis and centrifugation.

PROCEDURE

16. Place the dialysis tube (MWCO 3.5 kDA) in ultrapure water for 5 min.
17. Seal one end of the tube with a sealing clip and fill the tube with silk fibroin-LiBr solution.
18. Seal other end of the dialysis tube and fix this sealing clip onto a cork for the tube to flow in the water.
19. Dialyze against ultrapure water for 2 days. For efficient dialysis, use a large stir bar and place it on magnetic stirrer. Change water 6-8 times in the whole process.
20. Remove the solution from the dialysis tube and place it in a conical tube.
21. Centrifuge at 9000 rpm, 4 °C for 15 min to remove impurities and undissolved silk.
22. Carefully transfer the silk solution into the other tube using a pipette, leaving any impurity or undissolved silk behind.
23. Repeat steps 21 and 22.
24. Store the silk solution at 4 °C.

1.2.4 Precautions

- To avoid boiling over, add sodium carbonate slowly to the boiling water with constant stirring.
- Do not leave the beakers unattended while heating and boiling.
- Add LiBr to the silk, otherwise it will take much longer time to dissolve.
- Be careful not to puncture the dialysis tube.

1.3 Final product: aqueous fibroin solution

Final product of the protocol is a 7-10% (wt/vol) aqueous solution of the silk fibroin. Concentration of silk in the solution can be determined by taking a known volume (1 ml) of the

solution and drying it in the oven at 50 °C, then measuring the weight of the dried silk and dividing it by the volume.

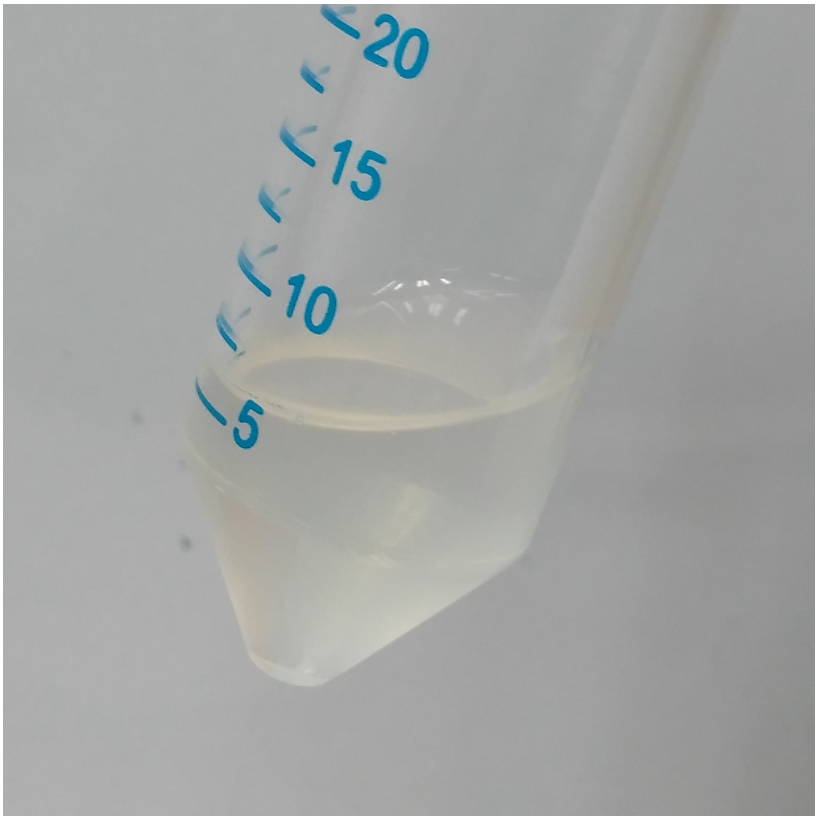

Figure 1.9: Final product is a clear 7-10% (wt/vol) aqueous solution of silk fibroin.

The solution is optically clear after dialysis and is more viscous than water (Figure 1.9). End products of steps I and II can be stored for long-term. But, the final solution can only be stored for about 45 days at 4 °C. After that the fibroin solution will become gel (Figure 1.10). Once the silk has gelled, it can not be used for material fabrication. For storing fibroin solution for more than 45 days, it can be lyophilized [4].

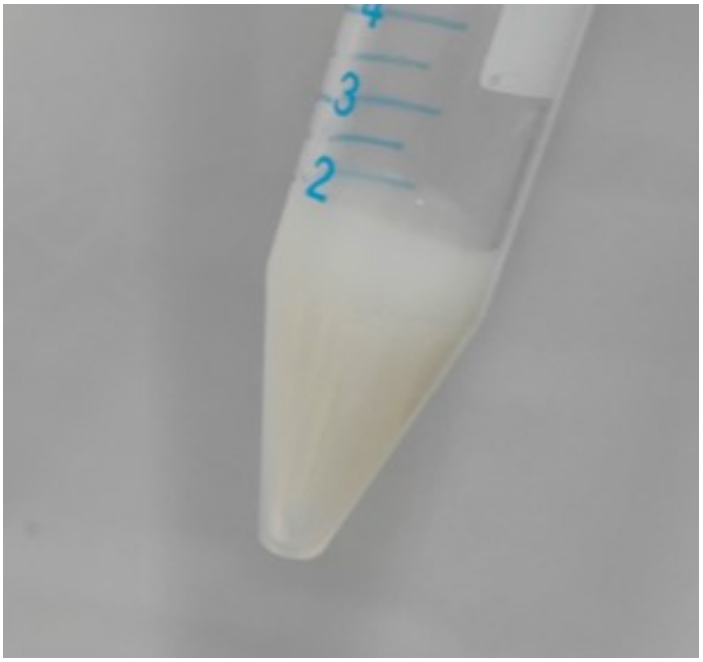

Figure 1.10: Degraded silk solution.

1.4 Conclusions

We have successfully reproduced the protocol and prepared an optically clear 7-10% (wt/vol) aqueous silk fibroin solution which can be stored at 4 °C for about 45 days. This solution can be used directly in fabrication of thin films, electrospun fibers, hydrogels sponges, etc [4]. Now that the silk fibroin solution has been prepared, next step is its characterization. In the next chapter, we have tried to investigate the structural changes in the silk caused by the degumming and dissolution and also tried to characterize silk using techniques like Raman spectroscopy, UV–visible spectroscopy and X-ray diffraction crystallography.

Chapter 2

Silk Characterization

2.1 Introduction

We used the silk fibroin solution prepared the previous chapter and tried to characterize the *Bombyx mori* using Raman spectroscopy, UV–visible spectroscopy and X-ray diffraction crystallography. We also tried to investigate the structural changes in the silk caused by the degumming and dissolution process. We studied the chemical and conformational structures of the *Bombyx mori* native silk fibers, degummed fibers, fibroin solution and the thin silk film prepared using the fibroin solution prepared in previous chapter using Raman spectroscopy. We also studied UV-Vis absorption spectrum of the fibroin solution. We used thin silk films to study its crystalline structure with the help of PXRD technique.

2.2 Optical characterization techniques

2.2.1 Raman spectroscopy

We used Raman spectroscopy to investigate the structural changes in the silk fibroin at different stages in the process of preparing the silk solution. We compared the Raman spectra of the cocoon silk fiber, degummed silk fiber, fibroin solution and the silk films prepared using the silk solution. In addition to conformational information, Raman spectroscopy also provides information about the secondary and tertiary structure of the proteins, therefore, it is a powerful tool for studying proteins. It is nondestructive and gives strong bands for aromatic structures which are present in some of the fibroin amino acids such as tyrosine, tryptophan, and phenylalanine [19]. Amide I and amide III vibrational bands provide the information on the secondary structure of the silk. Different types of secondary structures are characterized by amide I bands slightly different in position and shape. Amide III band gives complementary structural information on the protein structure, the structure of amide

III band can be correlated to the amide I band. Amide I and amide III vibrational modes [19, 20, 21, 22].

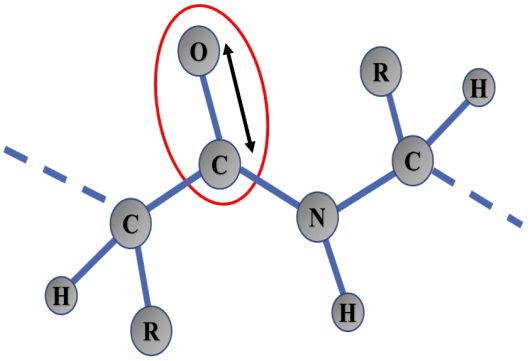

Figure 2.1: Amide I band: 80% C=O stretching, near 1650 cm^{-1}

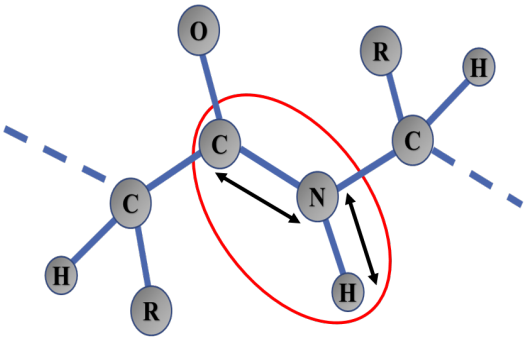

Figure 2.2: Amide III band: 40% C–N stretching, 30% N–H bending, near 1300 cm^{-1}

Raman Spectra of the silk at different stages in the protocol

We recorded Raman spectra of the cocoon fibers, degummed silk fibers and the fibroin solution using same laser and same parameters to investigate the conformational changes caused by the degumming and the dissolution process.

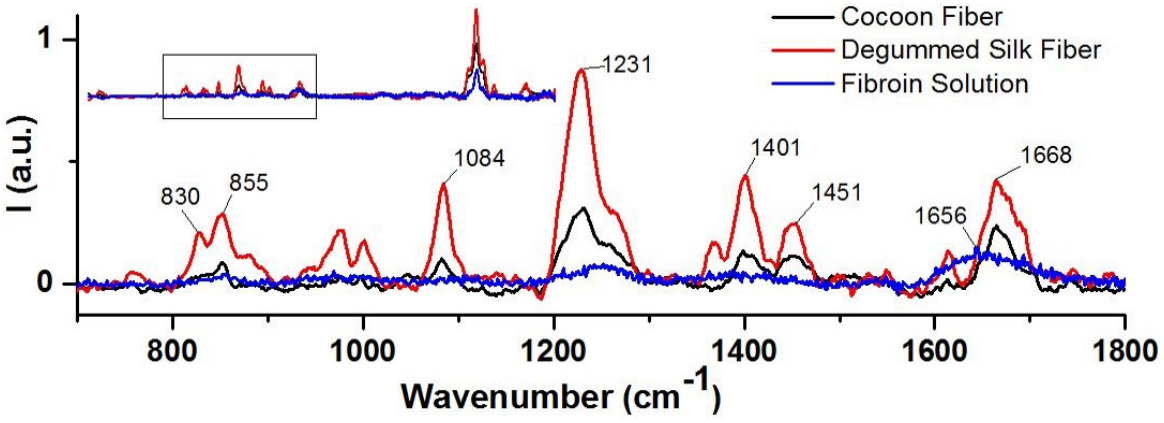

Figure 2.3: Raman Spectra of the cocoon silk fiber, degummed silk fiber and fibroin solution using 514 nm laser at 100× and 10 s exposure time.

Table 2.1: Raman peaks assignment for silk fibroin.

Wavenumber (cm^{-1})	Assignment
765	Tryptophan
830	Tyrosine
855	Tyrosine
1084	C-N Stretch, β-sheet
1231	Amide III, β-sheet
1271	Amide I, α-helix
1451	CH_2, CH_3 bending
1656	Amide I, α-helix
1668	Amide I, β-sheet
1685	Amide I, β-turn
2935	CH_3 asymmetric stretch
3066	C-N-H bond overturn

Raman peaks assignment for the spectra is shown in Table 2.1 [19, 20, 21]. Tyrosine peak at 855 cm^{-1} is present in all three spectra. Amide III peak at 1231 cm^{-1}, corresponding to the β-sheets is present in all three spectra. Amide III peak at 1271 cm^{-1} for the α-helix is only present in fibroin solution and is absent in the other two spectra. Amide I peak (1656 cm^{-1}) for the α-helix is present only in the fibroin solution not in the other spectra. Amide III peak, around 1668 cm^{-1}, corresponding to the β-sheets is absent in the fibroin solution but present in the other two spectra. The peak at 2935 cm^{-1} is present in all three spectra which corresponds to the CH_3 asymmetric stretch.

Raman spectra of the thin silk films

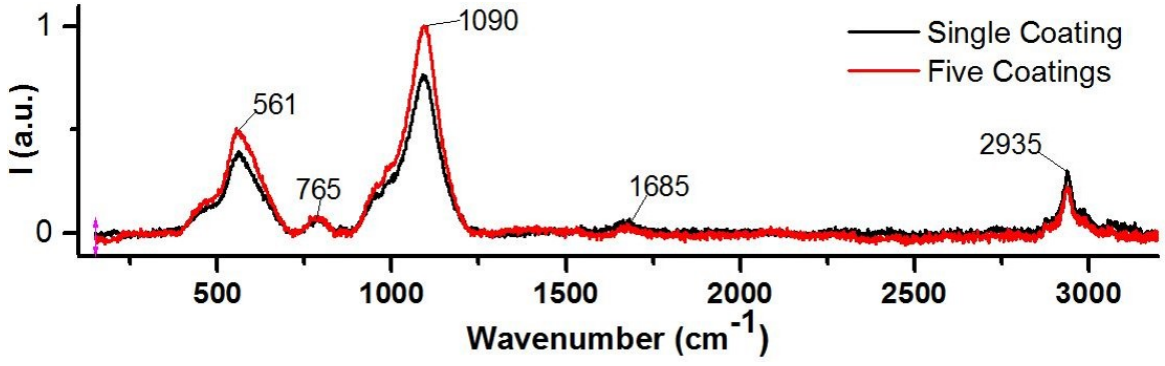

Figure 2.4: Raman Spectra of the spin coated thin silk films, prepared by single coating and by five coatings of the silk solution using 514 nm laser at 100× magnification and 10 s exposure time.

We prepared thin silk fibroin films by coating silk solution on the glass slide using spin-coater and drying the slide by placing it in the hot air oven at 50 °C after each coating for 10 min. We recorded Raman spectra of the silk films under the same conditions. C-N stretch, β-sheet peak at 1090 cm^{-1} is present in the silk films. This same is present at 1084 cm^{-1} in the Raman spectra of the cocoon fibers and degummed silk fibers. β-turn peak at 1085 cm^{-1} and CH_3 asymmetric stretch peak at 2935 cm^{-1} is also present in all the spectra.

2.2.2 Ultraviolet–visible spectroscopy

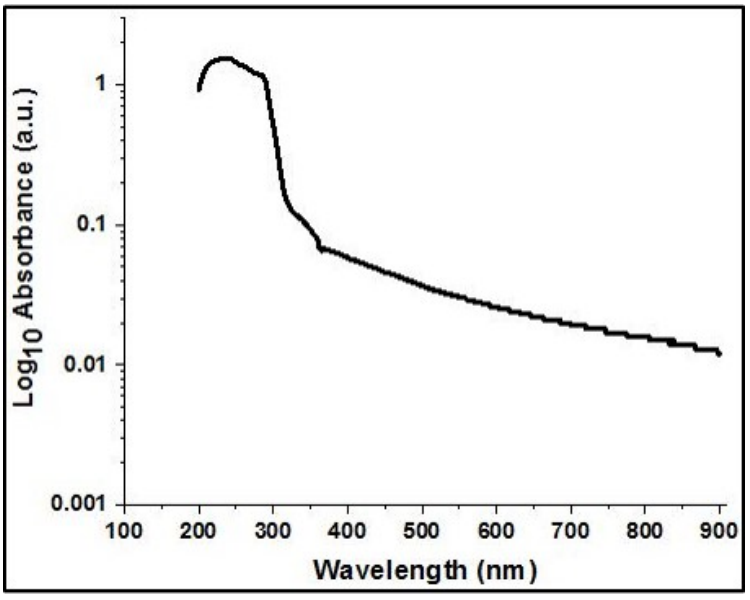

Figure 2.5: UV-Vis absorption spectrum of the silk fibroin solution.

UV-Visible absorption spectrum of the aqueous silk fibroin solution shows that it absorbs strongly in the middle UV region which is in accordance with the earlier reported results [23, 22].

2.2.3 X-ray diffraction crystallography

X-ray diffraction technique is an effective tool to classify a crystalline structure, but it is not as efficient for non-crystalline organic materials because peaks in their diffraction pattern are weak and broad. Hence to record the diffraction pattern, we prepared silk fibroin films by letting the solution dry in a petri dish at 45 °C.

Properties of silk fibroin can be easily modified can be modified by various treatments, such as, changing the crystalline content of the silk films by treating them with methanol [6] or by using water vapor annealing [4, 24]. We recorded the PXRD spectrum of the silk

fibroin films without any treatment and also of the water vapor annealed silk films to check the change in the crystalline structure of the fibroin by this treatment.

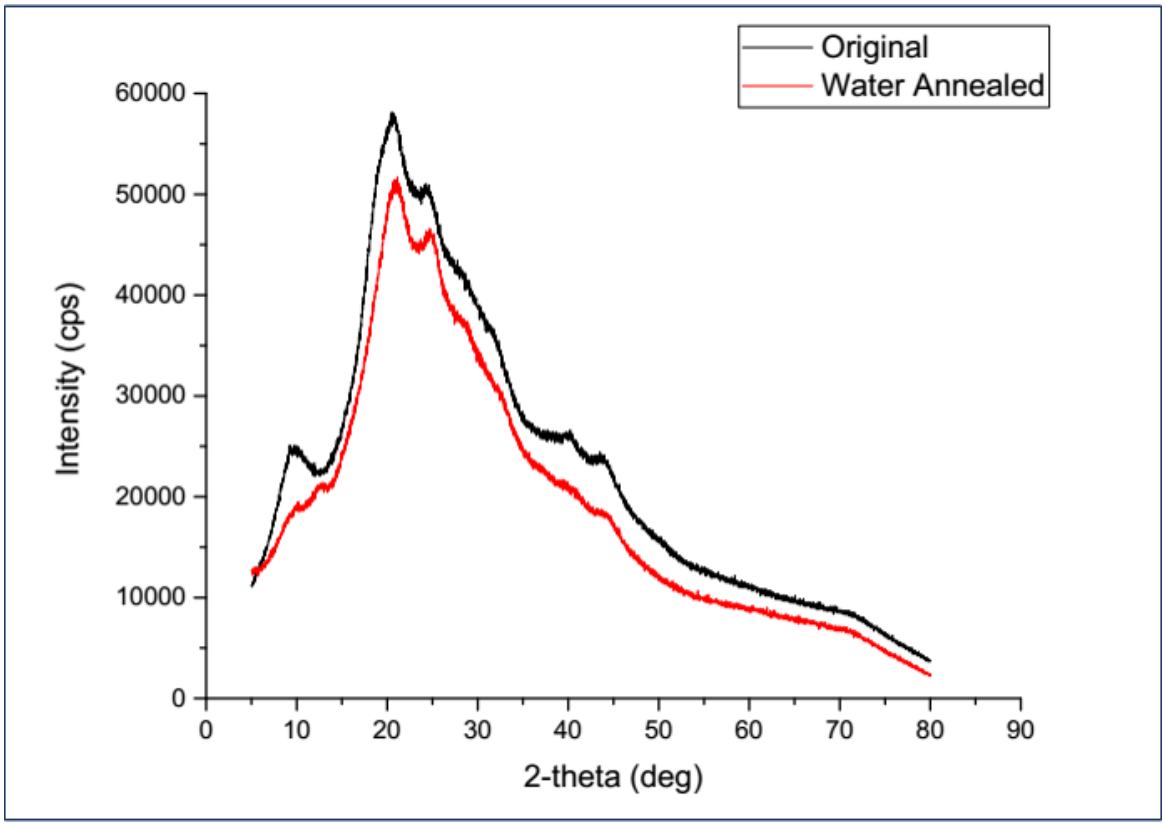

Figure 2.6: PXRD spectrum of the thin silk films using copper as the source of X-rays ($\lambda = 1.5406$ Å).

Table 2.2: Peaks in the PXRD spectrum of the silk fibroin film without any treatment and their respective lattice spacing, d.

2θ (deg)	**d (A°)**	**FWHM (deg)**	**Relative intensity**
9.14	9.67	2.67	3.80
10.00	8.84	3.21	12.00
20.32	4.37	5.09	100.00
24.47	3.63	3.40	31.31
27.40	3.25	4.90	32.91
31.75	2.82	4.80	18.30
40.32	2.24	4.90	7.97
44.03	2.06	4.90	4.87

Table 2.3: Peaks in the PXRD spectrum of the water annealed silk fibroin film and their respective lattice spacing, d.

2θ (deg)	**d (A$^\circ$)**	**FWHM (deg)**	**Relative intensity**
9.69	9.12	1.4	0.73
15.97	5.54	3.8	5.91
20.67	4.29	7.1	100.00
24.94	3.57	2.8	11.15
29.10	3.06	4.9	26.02
33.10	2.71	9.1	16.18

From the peaks in the PXRD spectrum, we calculated respective lattice spacing, d, listed in the Tables 2.2 and 2.3.

2.3 Conclusion

In this chapter. we used We used the silk fibroin solution prepared the previous chapter and tried to characterize the *Bombyx mori* using Raman spectroscopy, UV–visible spectroscopy and X-ray diffraction crystallography. However, to find various physical properties of the silk solution like thermal diffusivity and surface tension, we can not use these techniques.

Hence, for further optical studies, we have used pump-probe technique on LDI set-up which has a precision of about 5 nm [25, 26] to see if we could observe the radiation pressure effect and thermal effect of a high power laser beam on a droplet of the silk fibroin solution prepared in Chapter 1.

Chapter 3

Laser Induced Nanoscale Deformations in *Bombyx mori* Silk Solution

3.1 Inroduction

For further optical studies, we have used pump-probe technique on Liquid Drop Interferometer (LDI) set-up. [25, 26]. Using this technique, we tried to measure the radiation pressure effect and thermal effect of a high power laser beam on a drop of the silk fibroin solution prepared in Chapter 1. Advantages of this technique are its high precision (¡ 5nm) and self-calibration [25, 26]. By using this technique, we could be able to study the change in the physical properties of the silk solution real-time while it is drying.

3.1.1 Deformation due to the radiation pressure effect of a laser beam on air-liquid interface

Various studies have reported an outward bump on the air-liquid interface [27, 28, 29, 30, 26] which is in agreement with the prediction of the Minkowski momentum [31]. Minkowski predicted that photons would gain momentum $P' = nP$ compared to its value in vacuum P, upon entering a medium of refractive index, n. The Minowski's momentum corresponds to the wave nature of light. Momentum of photons is $P = h/\lambda$ and when it enters in a medium, its wavelength gets reduced by a factor of n and therefore, the momentum gets increased by the factor of n./par When a laser is made to incident on a liquid surface, due to this change in momentum, the interface gets deformed and by measuring the magnitude of this deformation, one can measure the surface tension of the liquid. [32].

3.1.2 Deformation due to thermal effect of the laser beam

When a Gaussian laser beam is incident on a liquid surface, it heats up the surface of liquid and induces a local variation in the interfacial tension which generates tangential shear stress and sets up hydrodynamic flows known as thermocapillary or Marangoni flows [33]. When the effective interfacial tension increases with temperature, the tangential stress is directed towards the heating spot, inducing a dimple on the surface. In the case, where the effective interfacial tension decreases with temperature, the tangential stress is directed from the hot region to the non-heated area of the interface and the direction of the flow is inverted forming a bump on the interface.

After shutting off the laser, the interface will relax back to its original position and if this relaxation is exponential, we can find the relaxation constant (t_{d}) and, in turn, calculate the thermal diffusivity α of the liquid by using the relation [34]:

$$t_{\mathrm{d}} = \frac{\omega^2}{4\alpha} \tag{3.1}$$

Where ω is the beam spot diameter when the inyensity falls by $\frac{1}{e^2}$.

3.2 Schematic of the experimental set-up

Silk drop is placed on a glass prism and a low power He-Ne laser is incident on the drop quasi-normally from above. The base diameter, w of the drop is around 5 mm and its central height is, $h = 1.0$ mm. Reflections from air-liquid and liquid-glass interface overlap to form Newton-ring like circular fringes as shown in figure 4.1. Due to evaporation of the silk drop, the central thickness of the drop, h(t) changes, thus producing a phase-shift. A photodiode an oscilloscope is simultaneously recording the intensity corresponding to the central fringe. Collapse of one fringe, i.e., from one central maximum to the next minimum of I(t), correspond to an optical path length change of $\lambda cos(\theta_{\mathrm{r}})/4n \approx 114nm$ for our experimental conditions (incident angle, $\theta_{\mathrm{i}} = 20°$). A high power pump laser beam is tightly focussed (spot size, ω =200 μm) normally on the drop from above and on the center of the probe laser beam spot. ON-OFF of pump laser beam is controlled using the shutter. We recorded data every minute till the drop is dry.

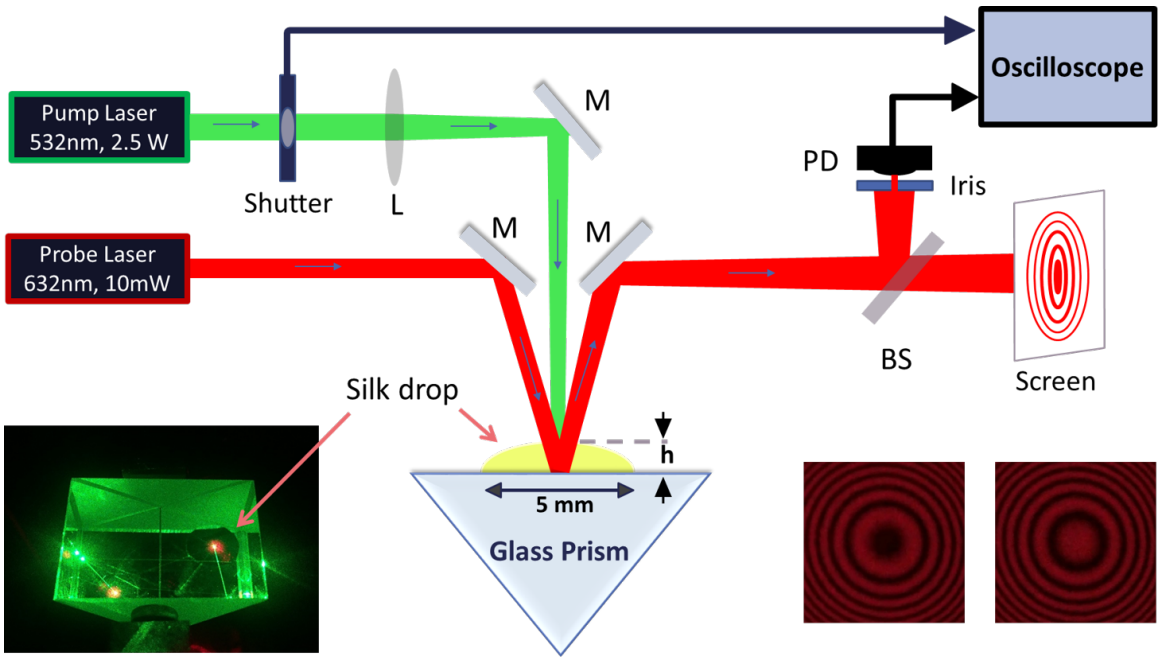

Figure 3.1: Schematic of the experimental set-up. A 15 μl, 0.5 cm diameter drop of the silk solution is placed on the glass prism. He-Ne probe laser beam ($\lambda = 632$ nm, 10 mW) is made to incident on the silk drop quasi-normally from above. A green pump laser beam ($\lambda = 532$ nm, 2.5 W) is focused on the air-liquid interface normally from above, controlled by a shutter. A photodiode (PD) is simultaneously capturing intensity I(t) of the central fringe. Inset: picture of the silk drop on the glass prism with both pump and probe laser beam are incident on.

3.3 Measuring the magnitude and direction of the deformation on the interface

- Direction of the deformation, or in other words, a bulge or a dimple at the interface is found out by checking whether the experimental plot is forward or backward in time with respect to the drop evaporation fit. As going forward in time, height of the drop is decreasing due to evaporation, therefore, if the experimental plot is forward in time with respect to the evaporation fit, it means that he height of the drop is decreased, i.e., a dip at the air-liquid interface and the other case means there is a bump.

- Magnitude of the deformation is calculated by measuring the intensity difference of the experimental data from the theoretical fit for the drop evaporation and comparing it with the intensity difference between the maxima and the minima, which corresponds to 114 nm as calculated in the previous section.

3.4 Results

We observed both radiation pressure effect and thermal effect on the silk drop using LDI technique. Due to radiation pressure there is a bulge at the interface, which is in agreement with Minkowski's momentum. But local heating by the laser beam is causing a dip at the air-liquid interface. The effect of radiation pressure is very fast but the thermal effect is slow and also persists for some time even after closing the shutter as the air-liquid interface relaxes back to its initial position.

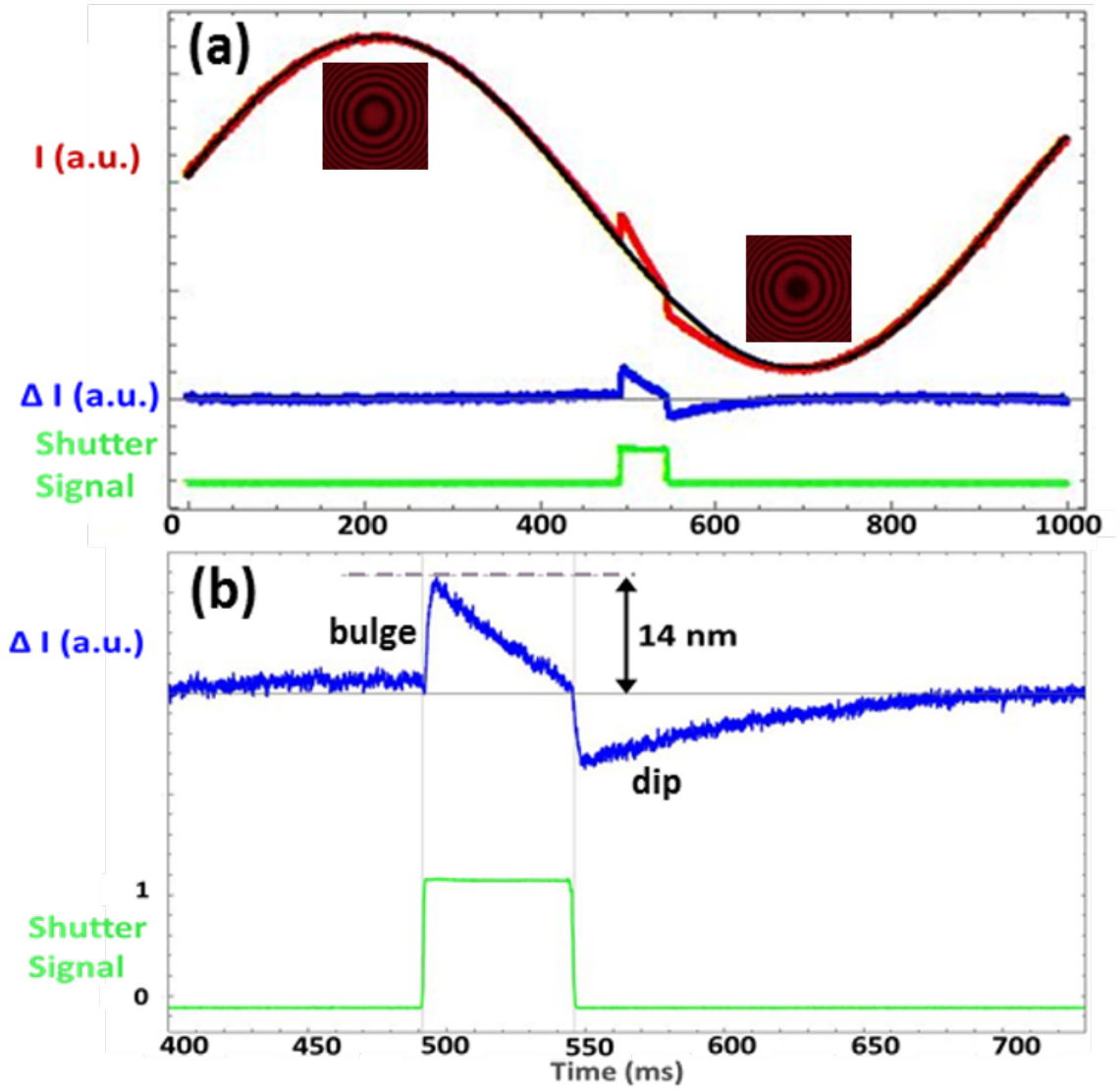

Figure 3.2: Plots of intensity I(t) versus time. Data acquired using PD and an oscilloscope after 1 min of placing the drop. Red line is the experimental data. Black line is the evaporation baseline, a $(I_{\mathrm{b}} + I_0 cos^2(ft + \phi))$ fit to the experimental data with fitting parameters: $I_b = 0.000552$, $I_0 = 0.006104$, $f = 3.265$ Hz, $\phi = 1.909$. Two snapshots of the interference pattern corresponding to maximum and minimum of I(t) are shown in the insets of (a). Blue line is the probe intensity after subtracting evaporation baseline from, ΔI. Green line is the simultaneously recorded shutter signals controlling the pump beam. (b) Is the zoom of ΔI and shutter signal with magnitude and direction of deformation labelled.

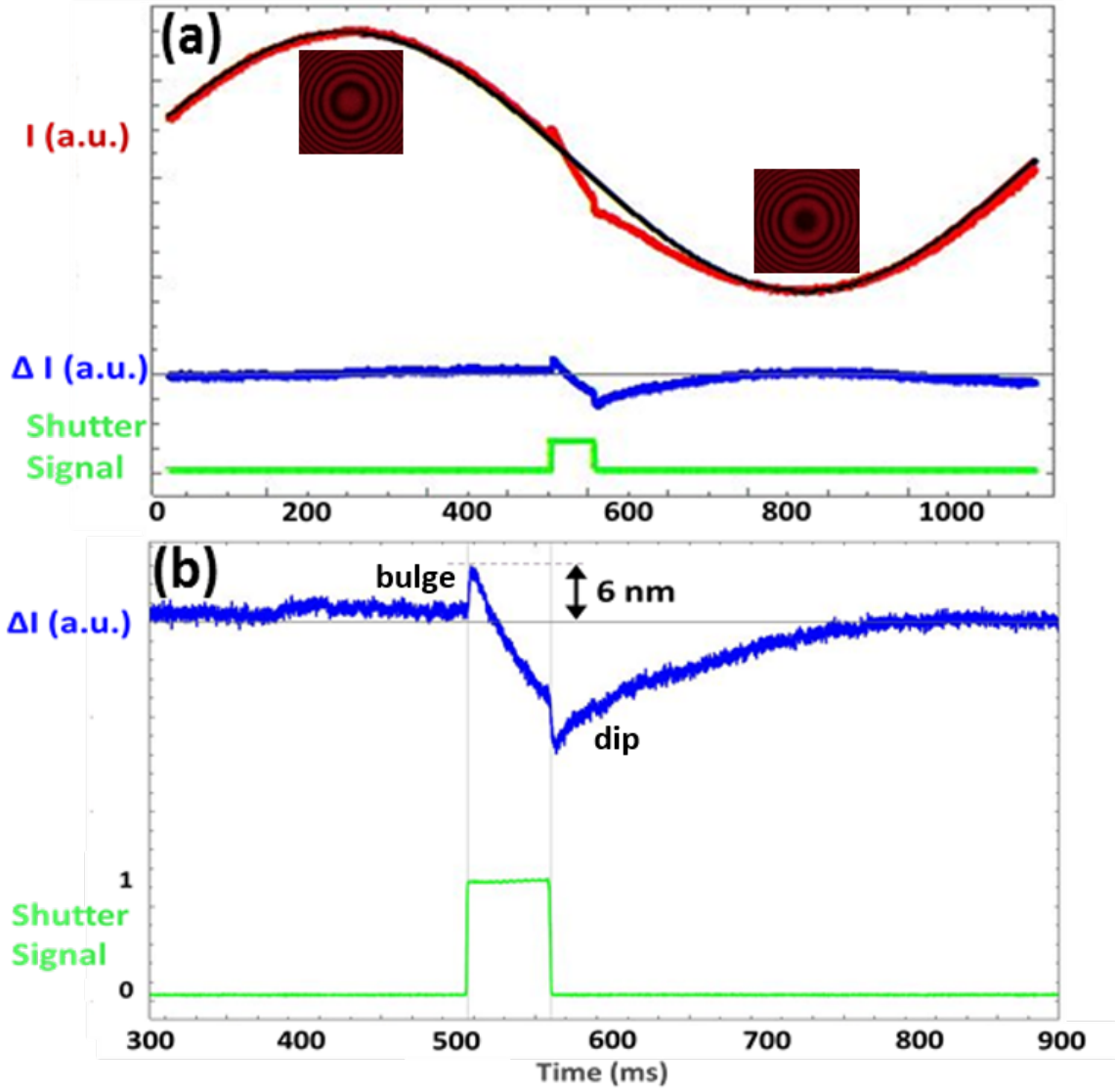

Figure 3.3: Plots of intensity I(t) versus time. Data acquired using PD and an oscilloscope after 6 min of placing the drop. Other plot details are same as in the Figure 3.2. Fitting parameters for the evaporation baseline are: $I_b = 0.001679$, $I_0 = 0.005268$, $f = 2.748$ Hz, $\phi = 1.92$.

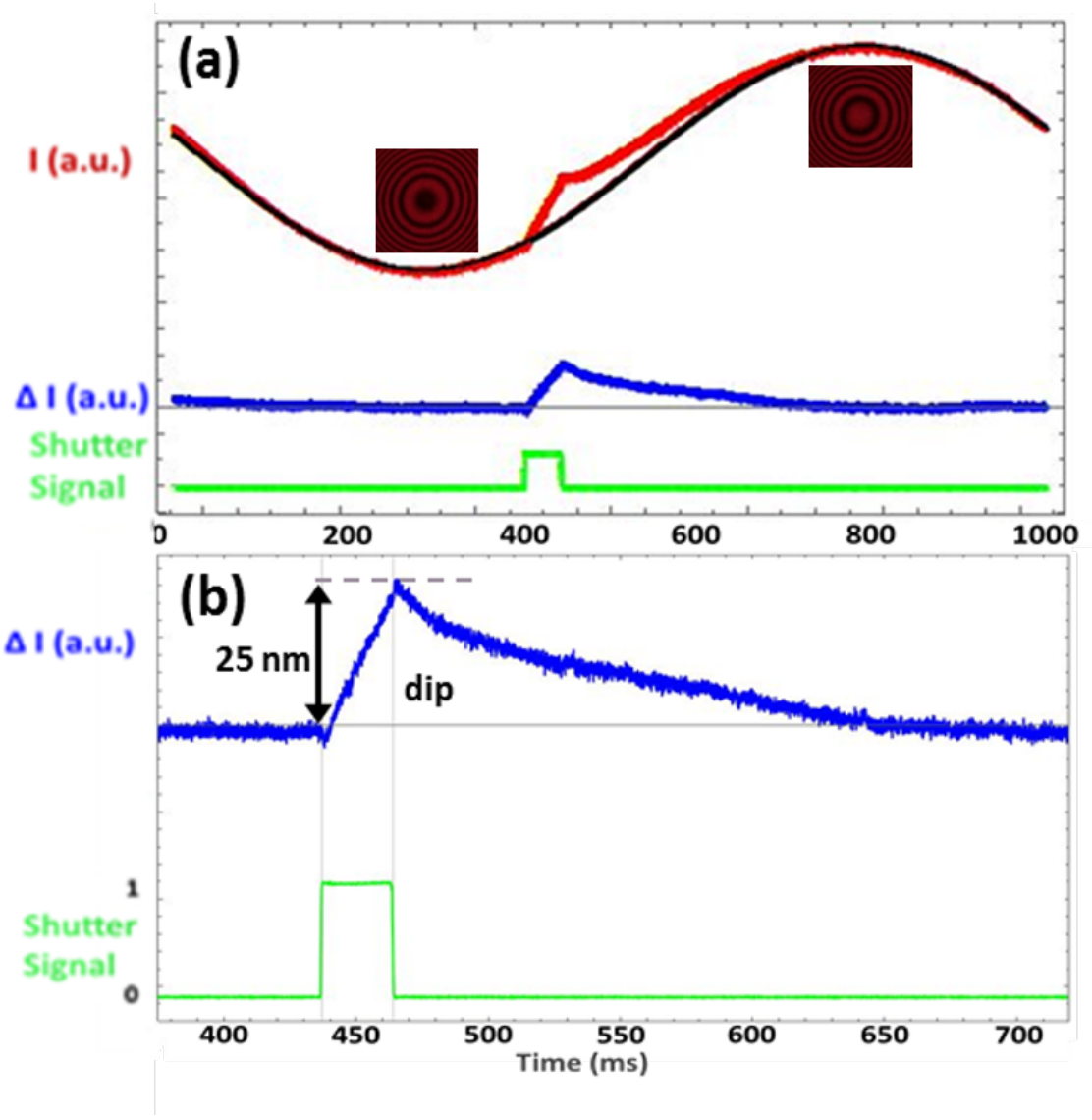

Figure 3.4: Plots of intensity I(t) versus time. Data acquired using PD and an oscilloscope after 12 min of placing the drop. Other plot details are same as in the Figure 3.2. Fitting parameters for the evaporation baseline are: $I_b = 0.00259$, $I_0 = 0.00427$, $f = 2.426$ Hz, $\phi = 3.204$.

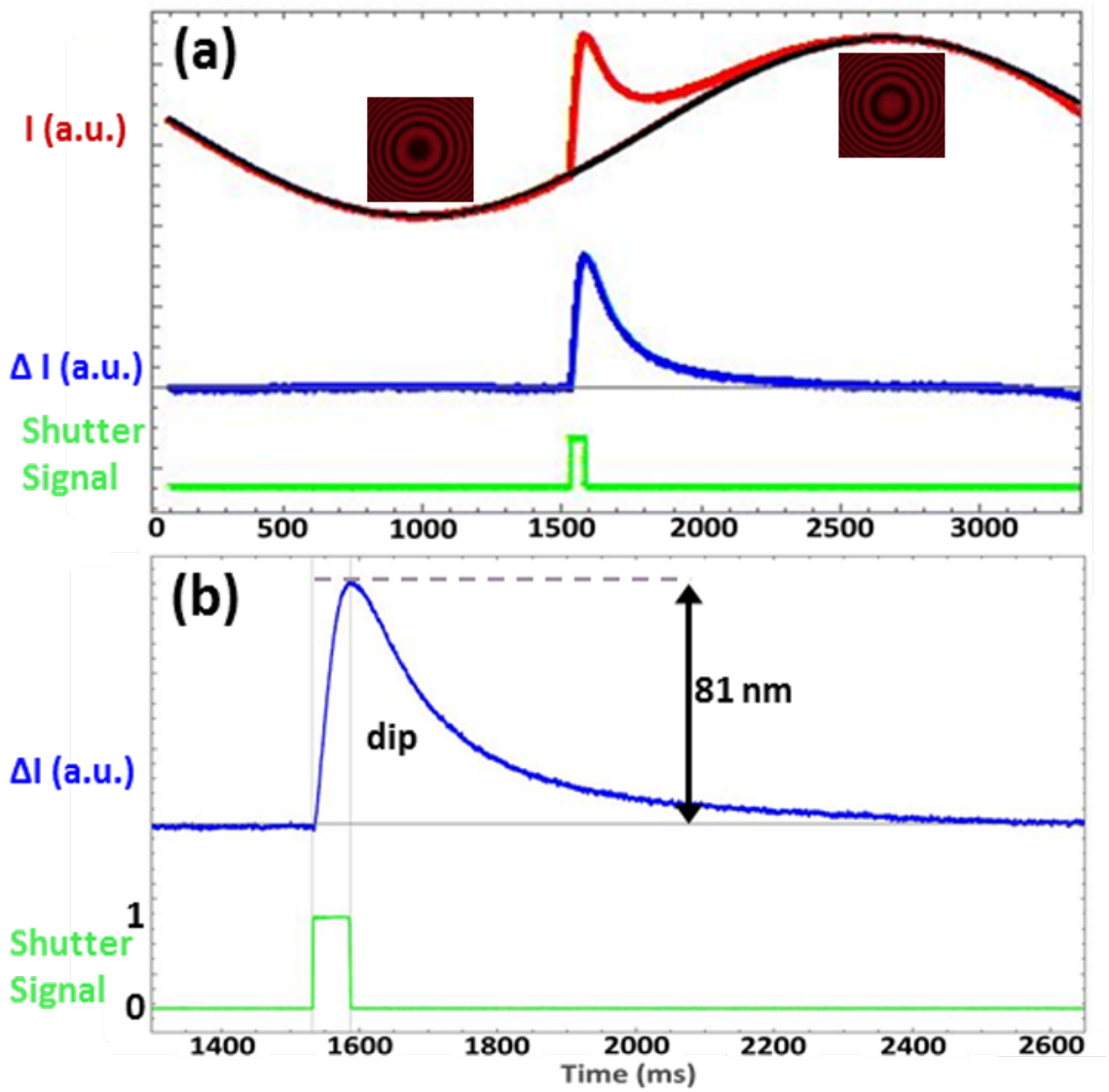

Figure 3.5: Plots of intensity I(t) versus time. Data acquired using PD and an oscilloscope after 25 min of placing the drop. Other plot details are same as in the Figure 3.2. Fitting parameters for the evaporation baseline are: $I_b = 0.001196$, $I_0 = 0.004392$, $f = 0.935$ Hz, $\phi = 2.515$.

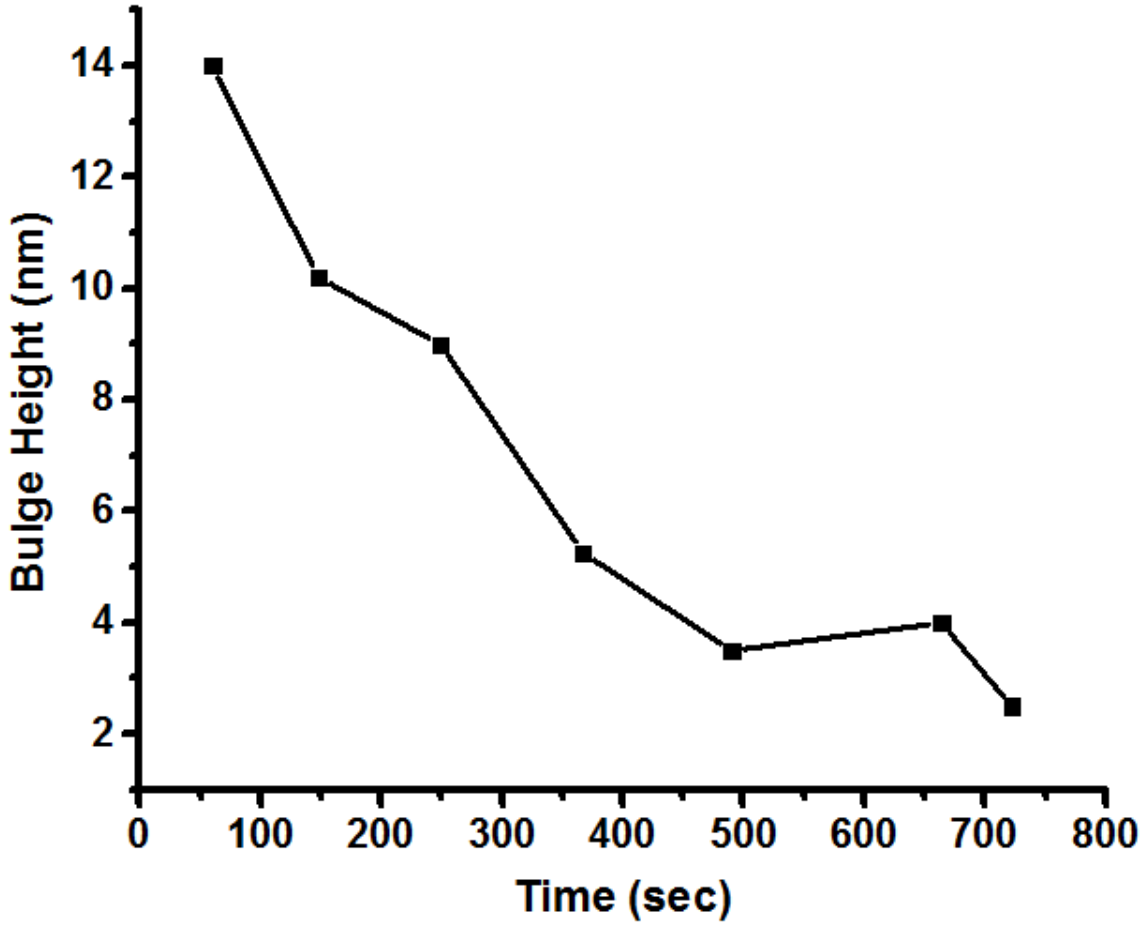

Figure 3.6: Plot of the height of the bulge due to radiation pressure effect verses time after placing the droplet on the prism.

Decrease in the bulge height due to the effect of radiation pressure suggests that the surface tension is increasing as the silk drop is getting more and more concentrated.

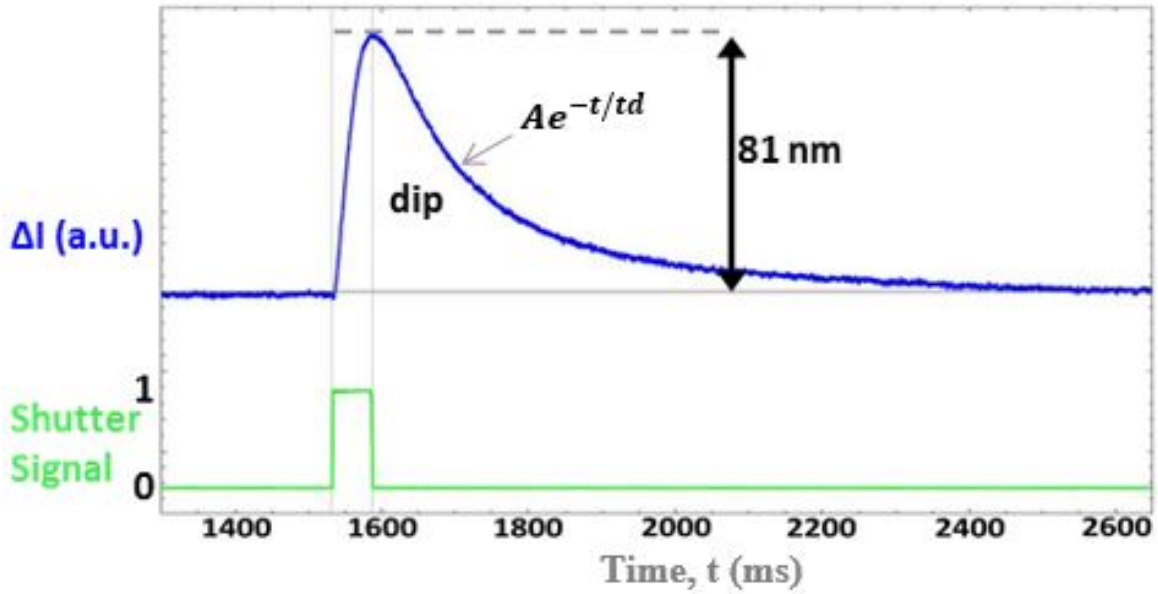

Figure 3.7: Relaxation in the interface due to the persisting thermal effect after the shutter is closed.

Relaxation in the interface due to the persisting thermal effect after the shutter is closed is fitted with exponential decay equation, Ae^{-t/t_d}, to find out the decay constant which, in turn, used to calculate thermal diffusivity by using the equation (3.1).

Table 3.1: Time constant and thermal diffusivity of the silk drop at different times after placing the drop.

Time (min)	**Time constant (t_d)**	**Thermal Diffusivity ($\times 10^{-9}$ m^2/s)**
1	0.0745	1.1636
4	0.1087	1.6988
11	0.0852	1.3312
15	0.0880	1.3752
18	0.0975	1.5228
20	0.1225	1.9144
22	0.1528	2.3871
25	0.1527	2.3866

3.5 Discussion

At the starting, just after placing the drop on the prism (Figure 3.2), the effect of radiation pressure is dominating and there is a bulge as long as the shutter is open and when the shutter is closed, the effect of radiation pressure shuts off and there is a dip at the air-liquid interface due to the thermal effect which relaxes back to the normal position. With time, due to evaporation, the silk drop is getting concentrating, and therefore, the effect of radiation pressure is decreasing and thermal effect is increasing as seen in the Figures 3.3, 3.4 and only the thermal effect was observed in the Figure 3.5. By studying the thermal effect, we calculated change in thermal diffusivity with the drying of drop. However, more data is needed to establish the results.

Chapter 4

General Conclusions and Future Perspectives

Silkworm silk is one of the most useful and oldest natural fiber in the world. It is highly regarded in the textile industry for its lustre and mechanical properties. People have been cultivating *Bombyx mori* silkworm for centuries. It has recently gained attention as a remarkable biomaterial and various scaffolds such as thin films, sponges, hydrogels, thin tubes, electrospun fibers have been processed from it which could have various biomedical applications.

In this study, we started by preparing an aqueous solution of the silk by removing sericin from the silkworm cocoons and dissolving the fibroin in LiBr. We obtained an optically clear 7-10% (wt/vol) aqueous solution of the silk fibroin. This whole protocol takes four days. One of the future aim will be to make this protocol faster, which could be done by searching for a better solvent or a better way to dissolve the fibroin as two out four days in the protocol is taken up in removing LiBr from the fibroin solution. Next aim is to find out a way by which we can quantitatively make sure that the sericin and LiBr are not present in the final solution. To prepare silk fibroin solution, sericin component must be removed from the core fibroin fibres.

In second chapter, we investigated structural changes caused by the degumming and dissolution process on the silk fibroin and characterized *Bombyx mori* silk fibroin by using techniques like Raman spectroscopy, UV–visible spectroscopy and X-ray diffraction crystallography. Raman spectra shows the presence of β-sheets in all the forms of the silk fibroin but the peak for α-helices was only observed in the case of liquid silk. Dominance of β-sheet regimes within the fibroin impart it with high mechanical strength.There is high absorption in the middle UV region. Crystalline index of the silk films was found to be around 20 %. Future aim is to use Circular dichroism (CD) to find more details about the secondary structure of the fibroin.

In third chapter, we used pump-probe technique on Liquid Drop Interferometer set-up on silk drop. We observed both radiation pressure effect, in agreement with Minkowski's momentum, and thermal effect on the silk drop. We calculated change in surface tension and thermal diffusivity of the silk with the drying of drop. Decrease in the deformation due to the radiation pressure effect suggested the surface tension is increasing as the drop is getting concentrated. Our preliminary results suggest that the thermal diffusivity of the silk solution was less as compared to the water. However, we need to take more data with different experimental conditions to establish the results.

Appendix A

Materials required for silk solution preparation protocol

- **Reagents used in the protocol**
  - *Bombyx mori* silk cocoons
  - Sodium Carbonate (HiMedia)
  - Ultrapure water
  - Lithium Bromide (HiMedia)

- **Equipment used in the protocol**
  - Glass beakers
  - Aluminum foil
  - Spatula
  - Magnetic stirrer with hot plate
  - Magnetic beads
  - Magnetic bead retriever
  - Weighing balance
  - Scissors
  - Measuring cylinder
  - Glass bottle
  - Conical tubes
  - Micropipettes

- Micropipette tips
- Eppendorf tubes
- Dialysis tube (MWCO 3.5 kDA)
- Sealing clips
- Centrifuge
- 4 °C refrigerator

Appendix B

Water vapor annealing set-up

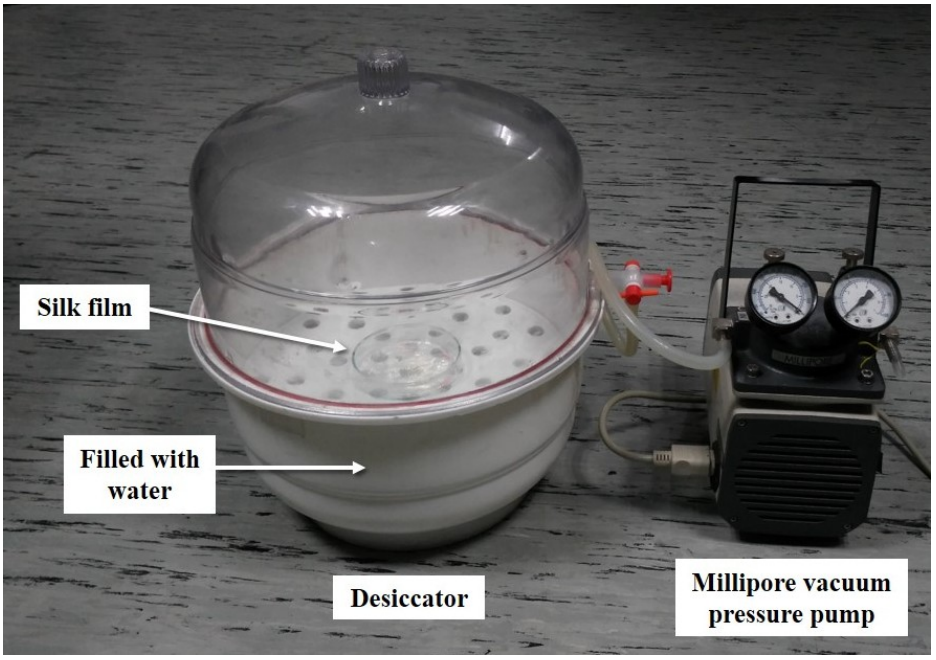

Figure B.1: Set-up for the water annealing of the silk fibroin films

Place the silk films in the desiccator and fill the bottom of the desiccator with water. Connect it to the vacuum pressure pump. After the vacuum is generated, close the vacuum port. The desiccator will get filled with water vapors. Leave the films in the desiccator for 6 h.

Bibliography

[1] N. Minoura, M. Tsukada, and M. Nagura, "Physico-chemical properties of silk fibroin membrane as a biomaterial," *Biomaterials*, vol. 11, no. 6, pp. 430–434, 1990.

[2] N. Minoura, M. Tsukada, and M. Nagura, "Fine structure and oxygen permeability of silk fibroin membrane treated with methanol," *Polymer*, vol. 31, no. 2, pp. 265–269, 1990.

[3] B. D. Lawrence, F. Omenetto, K. Chui, and D. L. Kaplan, "Processing methods to control silk fibroin film biomaterial features," *Journal of Materials Science*, vol. 43, no. 21, p. 6967, 2008.

[4] D. N. Rockwood, R. C. Preda, T. Yucel, X. Wang, M. L. Lovett, and D. L. Kaplan, "Materials fabrication from bombyx mori silk fibroin," *Nat. Protocols*, vol. 6, pp. 1612–1631, Sep 2011.

[5] T. Arai, G. Freddi, R. Innocenti, and M. Tsukada, "Biodegradation of bombyx mori silk fibroin fibers and films," *Journal of Applied Polymer Science*, vol. 91, no. 4, pp. 2383–2390, 2004.

[6] M. Tsukada, Y. Gotoh, M. Nagura, N. Minoura, N. Kasai, and G. Freddi, "Structural changes of silk fibroin membranes induced by immersion in methanol aqueous solutions," *Journal of Polymer Science Part B: Polymer Physics*, vol. 32, no. 5, pp. 961–968, 1994.

[7] R. L. Horan, K. Antle, A. L. Collette, Y. Wang, J. Huang, J. E. Moreau, V. Volloch, D. L. Kaplan, and G. H. Altman, "In vitro degradation of silk fibroin," *Biomaterials*, vol. 26, no. 17, pp. 3385–3393, 2005.

[8] W. A. Shear, J. M. Palmer, J. A. Coddington, and P. M. Bonamo, "A devonian spinneret: early evidence of spiders and silk use," *Science*, vol. 246, no. 4929, p. 479, 1989.

[9] F. Chen, D. Porter, and F. Vollrath, "Structure and physical properties of silkworm cocoons," *J R Soc Interface*, vol. 9, pp. 2299–2308, Sep 2012.

[10] E. S. Sashina, A. M. Bochek, N. P. Novoselov, and D. A. Kirichenko, "Structure and solubility of natural silk fibroin," *Russian Journal of Applied Chemistry*, vol. 79, no. 6, pp. 869–876, 2006.

[11] R. Valluzzi and S. P. Gido, "The crystal structure of bombyx mori silk fibroin at the air–water interface," *Biopolymers*, vol. 42, no. 6, pp. 705–717, 1997.

[12] T. Lefèvre, M.-E. Rousseau, and M. Pézolet, "Protein secondary structure and orientation in silk as revealed by raman spectromicroscopy," *Biophysical journal*, vol. 92, no. 8, pp. 2885–2895, 2007.

[13] Y. Takahashi, M. Gehoh, and K. Yuzuriha, "Crystal structure of silk (bombyx mori)," *Journal of Polymer Science Part B: Polymer Physics*, vol. 29, no. 7, pp. 889–891, 1991.

[14] N. D. Lazo and D. T. Downing, "Crystalline regions of bombyx mori silk fibroin may exhibit $\hat{I}^2$-turn and $\hat{I}^2$-helix conformations," *Macromolecules*, vol. 32, no. 14, pp. 4700–4705, 1999.

[15] D. S. Dwyer, "Molecular simulation of the effects of alcohols on peptide structure," *Biopolymers*, vol. 49, no. 7, pp. 635–645, 1999.

[16] R. Valluzzi, S. P. Gido, W. Muller, and D. L. Kaplan, "Orientation of silk iii at the air-water interface," *International journal of biological macromolecules*, vol. 24, no. 2, pp. 237–242, 1999.

[17] H.-J. Jin and D. L. Kaplan, "Mechanism of silk processing in insects and spiders," *Nature*, vol. 424, pp. 1057–1061, Aug 2003.

[18] S. Keten, Z. Xu, B. Ihle, and M. J. Buehler, "Nanoconfinement controls stiffness, strength and mechanical toughness of [beta]-sheet crystals in silk," *Nat Mater*, vol. 9, pp. 359–367, Apr 2010.

[19] J. Shao, J. Zheng, J. Liu, and C. Carr, "Fourier transform raman and fourier transform infrared spectroscopy studies of silk fibroin," *Journal of Applied Polymer Science*, vol. 96, no. 6, pp. 1999–2004, 2005.

[20] P. Monti, G. Freddi, A. Bertoluzza, N. Kasai, and M. Tsukada, "Raman spectroscopic studies of silk fibroin from bombyx mori," *Journal of Raman Spectroscopy*, vol. 29, no. 4, pp. 297–304, 1998.

[21] P. Monti, P. Taddei, G. Freddi, T. Asakura, and M. Tsukada, "Raman spectroscopic characterization of bombyx mori silk fibroin: Raman spectrum of silk i," *Journal of Raman Spectroscopy*, vol. 32, no. 2, pp. 103–107, 2001.

[22] W. I. Abdel-Fattah, N. Atwa, and G. W. Ali, "Influence of the protocol of fibroin extraction on the antibiotic activities of the constructed composites," *Progress in Biomaterials*, vol. 4, no. 2, pp. 77–88, 2015.

[23] K. Setoyama, "Studies on silk yellowing," *The Journal of Sericultural Science of Japan*, vol. 45, no. 4, pp. 351–357, 1976.

[24] X. Hu, K. Shmelev, L. Sun, E.-S. Gil, S.-H. Park, P. Cebe, and D. L. Kaplan, "Regulation of silk material structure by temperature-controlled water vapor annealing," *Biomacromolecules*, vol. 12, pp. 1686–1696, May 2011.

[25] G. Verma and K. P. Singh, "Universal long-range nanometric bending of water by light," *Phys. Rev. Lett.*, vol. 115, p. 143902, Oct 2015.

[26] G. Verma, K. Chaudhary, and K. P. Singh, "Nanomechanical effects of light unveil photons momentum in medium," *Scientific Reports*, vol. 7, pp. 42554 EP –, Feb 2017. Article.

[27] A. Ashkin and J. Dziedzic, "Radiation pressure on a free liquid surface," *Physical Review Letters*, vol. 30, no. 4, p. 139, 1973.

[28] A. Casner and J.-P. Delville, "Laser-induced hydrodynamic instability of fluid interfaces," *Physical review letters*, vol. 90, no. 14, p. 144503, 2003.

[29] E. Brasselet, R. Wunenburger, and J.-P. Delville, "Liquid optical fibers with a multistable core actuated by light radiation pressure," *Physical review letters*, vol. 101, no. 1, p. 014501, 2008.

[30] N. Bertin, H. Chraibi, R. Wunenburger, J.-P. Delville, and E. Brasselet, "Universal morphologies of fluid interfaces deformed by the radiation pressure of acoustic or electromagnetic waves," *Physical review letters*, vol. 109, no. 24, p. 244304, 2012.

[31] H. Minkowski, "Die grundgleichungen für die elektromagnetischen vorgänge in bewegten körpern," *Nachrichten von der Gesellschaft der Wissenschaften zu Göttingen, Mathematisch-Physikalische Klasse*, vol. 1908, pp. 53–111, 1908.

[32] K. Sakai, D. Mizuno, and K. Takagi, "Measurement of liquid surface properties by laser-induced surface deformation spectroscopy," *Physical Review E*, vol. 63, no. 4, p. 046302, 2001.

[33] H. Chraïbi and J.-P. Delville, "Thermocapillary flows and interface deformations produced by localized laser heating in confined environment," *Physics of Fluids*, vol. 24, no. 3, p. 032102, 2012.

[34] C. A. Carter and J. M. Harris, "Comparison of models describing the thermal lens effect," *Appl. Opt.*, vol. 23, pp. 476–481, Feb 1984.